AGU PUBLICATIONS

JGR

Journal of Geophysical Research: Space Physics

RESEARCH ARTICLE
10.1002/2016JA023346

Special Section:
Geospace system responses to the St. Patrick's Day storms in 2013 and 2015

Ionosphere data assimilation modeling of 2015 St. Patrick's Day geomagnetic storm

C. H. Chen[1], C. H. Lin[1], T. Matsuo[2,3], and W. H. Chen[1]

[1]Department of Earth Sciences, National Cheng Kung University, Tainan, Taiwan, [2]Cooperative Institute for Research in Environmental Sciences, University of Colorado Boulder, Boulder, Colorado, USA, [3]Space Weather Prediction Center, National Oceanic and Atmospheric Administration, Boulder, Colorado, USA

Key Points:
- First time to assimilate the GPSTEC observations with different high-latitude convection models in the TIEGCM
- Results show the latitudinal effect on the regional RMSEs and the capability of TEC forecast time
- The ionospheric assimilation system improves the storm time eastward electric fields

Correspondence to:
C. H. Lin,
charles@mail.ncku.edu.tw

Citation:
Chen, C. H., C. H. Lin, T. Matsuo, and W. H. Chen (2016), Ionosphere data assimilation modeling of 2015 St. Patrick's Day geomagnetic storm, *J. Geophys. Res. Space Physics*, *121*, 11,549–11,559, doi:10.1002/2016JA023346.

Received 15 AUG 2016
Accepted 6 NOV 2016
Accepted article online 11 NOV 2016
Published online 28 NOV 2016

Abstract The ionospheric plasma disturbances during a severe storm can affect human activities and systems, such as navigation and HF communication systems. Therefore, the forecast of ionospheric electron density is becoming an important topic recently. This study is conducted with the ionospheric assimilation model by assimilating the total electron content observations into the thermosphere-ionosphere coupling model with different high-latitude ionospheric convection models, Heelis and Weimer, and further to forecast the variations of ionospheric electron density during the 2015 St. Patrick's Day geomagnetic storm. The forecast capabilities of these two assimilation models are evaluated by the root-mean-square error values in different regions to discuss its latitudinal effects. Results show the better forecast in the electron density at the low-latitude region during the storm main phase and the recovery phase. The well reproduced eastward electric field at the low-latitude region by the assimilation model reveals that the electric fields may be an important factor to have the contributions on the accuracy of ionospheric forecast.

1. Introduction

Data assimilation technology, recently, has been employed on the forecast of ionospheric electron density during the geomagnetic storm conditions. Observations are assimilated into a physical model to adjust the model initial conditions for a better forecast accuracy. The dense of ground-based GPS networks provides continuous and wide-coverage observations of global total electron content (TEC). *Solomentsev et al*. [2014] performed GPSTEC assimilation for the September 2011 storm and validated their nowcast results by FORMOSAT-3/COSMIC. *Chartier et al*. [2016] and *Chen et al*. [2016] assimilated the GPSTEC observations into a theoretical numerical model (Thermosphere-Ionosphere-Electrodynamics General Circulation Model, TIEGCM) and further evaluated their effects on the storm time ionospheric electron density forecast. Since the rapidly dynamic changes of electric field, auroral particle precipitation, and Joule heating during storms, it is a challenge to capture the response to geomagnetic storms [*Fuller-Rowell et al*., 2004]. *Chen et al*. [2016] examined the effects of various assimilation cycle lengths on the ionospheric TEC forecast and suggested that the rapid cycling ionospheric data assimilation system is necessary for assimilation of various state variables during the storm period to capture the corresponding variations in time. They further found, even without accurate model driver specification, the frequently assimilation can restrain the overfitting effect during the storm conditions.

How to improve the forecast accuracy is another issue. An experiment test by *Chartier et al*. [2013] showed that the forecast accuracy can be maintained for just few hours if only the electron densities are updated in the assimilation model. Their results also showed that the updating of neutral parameters in the assimilation model, especially the neutral composition, is important to maintain the accuracy of ionospheric electron density forecast for over 18 h during the storm conditions. *Chen et al*. [2016] further indicated that updating neutral state variable in the assimilation step is an important factor in improving the trajectory of model forecasting, especially during the period of storm recovery phase. Because the neutral atmosphere components take longer time to recover from their updated states, in other words, they have a longer memory than the ionized components of ionosphere relatively [*Jee et al*., 2007]. Accordingly, the updated neutral state variables in the assimilation model can modify and affect the ionospheric electron density in a longer period.

It is also expected that the capability of physical model will directly influence the forecast accuracy. During storm times, the high energy deposits into the ionosphere and then causes the electric field variations, Joule heating, and ionization at high latitudes. TIEGCM adopts two empirical models, Heelis [*Heelis et al*.,

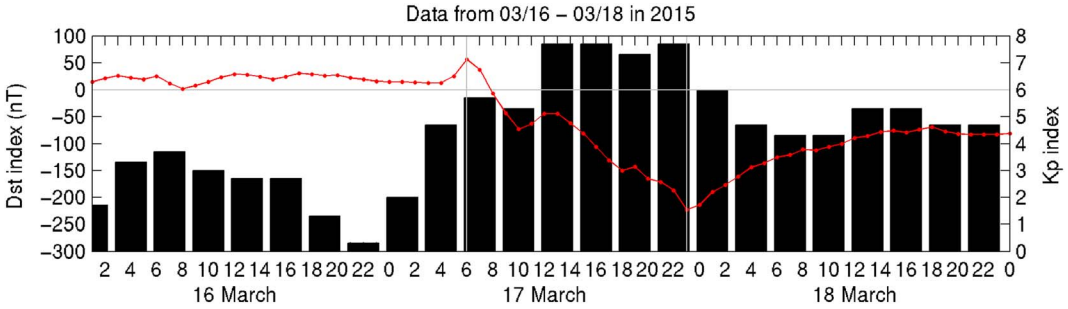

Figure 1. Time evolutions of *Dst* index (red dotted line) and *Kp* index (black bar) during 16–18 March 2015. The white vertical lines indicate the time at 0600 UT and 2300 UT, which the *Dst* index reaches its maximum and minimum values, respectively.

1982] and Weimer [*Weimer*, 2005], to calculate the high-latitude ion convection. The Heelis is the default model in TIEGCM and have been used to investigate its capability of ionospheric forecast during storm condition [*Chen et al*., 2016]. In this study, we adopt the same assimilation scheme outlined by *Chen et al*. [2016], but further employ the Weimer model in the TIEGCM to compare with the results by the Heelis model. The goal of this paper is to reproduce and forecast global TEC distribution during 2015 St. Patrick's Day storm and then further evaluate the ionospheric forecast performances of this assimilation system.

2. Assimilation Model Description

In this study, the ground-based GPSTEC observations during storm period are assimilated into the thermosphere-ionosphere coupling model, TIEGCM, by using an ensemble Kalman filter (EnKF) data assimilation system (Data Assimilation Research Testbed, DART [*Anderson et al*., 2009]), called DART/TIEGCM assimilation system. The solar UV and EUV fluxes in this model are parameterized according to the solar $F_{10.7}$ daily index. In order to create the 90 ensembles for EnKF, the Gaussian distributions of $F_{10.7}$ index are given by the width of $\pm 20\ 10^{-22}\,\mathrm{W\,m^{-2}Hz^{-1}}$ [cf. *Chen et al*., 2016]. The $F_{10.7}$ index during the nowcast and forecast periods are employed from the geophysical index inputs to DART/TIEGCM. In this study, we have conducted DART/TIEGCM simulations with high-latitude drivers from Heelis and Weimer models to determine the high-latitude ion convection, which are named as DART/TIEGCM-Heelis (DTH) and DART/TIEGCM-Weimer (DTW) hereafter. The Heelis model is driven by the *Kp* index, while the Weimer model is based on the interplanetary magnetic field (IMF) conditions. The ensemble spread (Gaussian distribution) of drivers in these two models is ± 1 unit for the *Kp* index and 20% of daily maximum value for the IMF parameters, respectively. The model state variables, neutral temperature, atomic and molecular oxygen mixing ratios (O, O_2), neutral winds, and atomic oxygen ion density (O^+), as well as electron density are included in the state vector of the DART/TIEGCM data assimilation system. The GPSTEC observations are assimilated into this assimilation scheme every 10 min. Noted that the time resolution of GPSTEC is 30 s and we accumulate the 10 min data for each assimilation cycle. Therefore, the ionospheric feature with the time scale less than 10 min may not be well captured. A horizontal localization function with the half width of 1,000 km is employed in this assimilation system to adjust the unobserved state variables but without employing the localization function in vertical direction.

2.1. Assimilation Results of 2015 St. Patrick's Day Storm

The St. Patrick's Day storm occurred on 17 March 2015, which the *Dst* index reaches its minimum of −223 nT around 2300 UT and the *Kp* index reaches its maximum of 7+ between 1200 and 1700 UT during the storm main phase as shown in Figure 1. There are strong positive and negative effects occurring at various longitude sectors producing remarkable TEC deviations and irregularities, which also lead to positioning errors [cf. *Astafyeva et al*., 2015; *Cherniak and Zakharenkova*, 2015; *Nava et al*., 2016; *Jacobsen and Andalsvik*, 2016]. The global TEC comparison of GPSTEC observations, model control run (TIEGCM without data assimilation), and the assimilation results (DTH and DTW) at 1600 UT on 17 March 2015 are shown in Figure 2. It is clearly seen that the storm enhanced density (SED) structure is observed by GPSTEC around the north part of North Atlantic. The TIEGCM control runs also reproduce this SED structure by using Heelis and Weimer

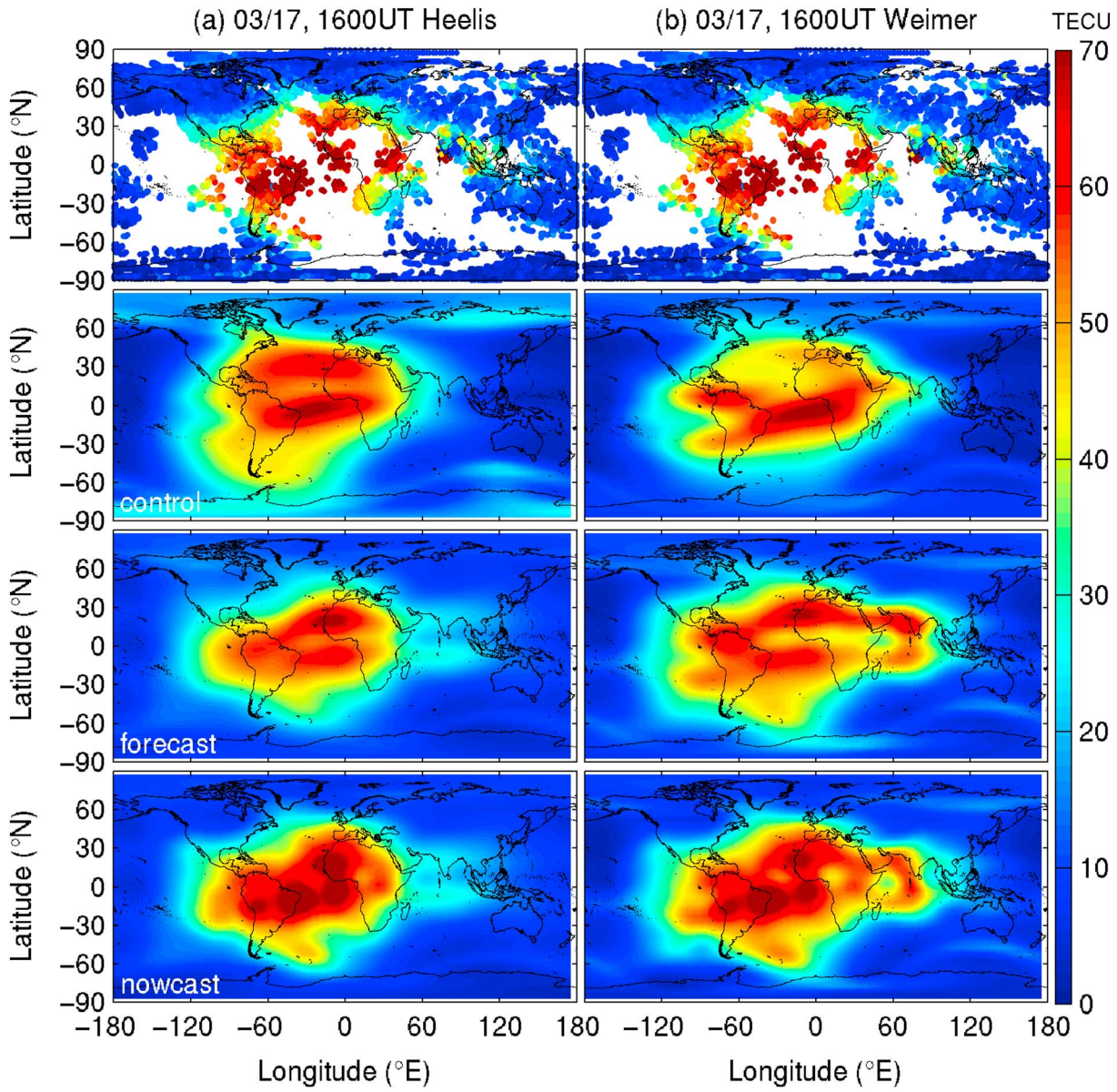

Figure 2. Global TEC map at 1600 UT on 17 March 2015 by (a) DART/TIEGCM-Heelis and (b) DART/TIEGCM-Weimer models. The top to bottom rows are the (first row) ground-based GPSTEC observations, (second row) TIEGCM without data assimilation (control run), (third row) prior TEC of data assimilation (forecast), and (fourth row) posterior TEC of data assimilation (nowcast), respectively. The unit of TEC is total electron content unit (1 TECU = 10^{16} el/m^2).

models, although the SED location is closer to the east coast of North American (second panels of Figures 2a and 2b). After assimilating GPSTEC, not only the SED location but also the strength of equatorial ionization anomaly (EIA) are adjusted to approach the observations (fourth panels of Figures 2a and 2b). The SED structure disappears in the forecast stage of the DTH model but is well reproduced by the DTW model (third panels of Figures 2a and 2b).

The root-mean-square error (RMSE) values are calculated to evaluate the performance of data assimilation system in different regions. The RMSE is defined as the differences between the modeled TECs (TIEGCM or DART/TIEGCM) and the actual observation (GPSTEC) [cf. *Chen et al.*, 2016]. The RMSEs are further separated as three regions by the magnetic latitudes and shown in Figure 3. At the high-latitude region (Figures 3a and 3b), the control RMSEs (gray-line) by the DTH model are smaller than those by the DTW model before 0500 UT on 17 March (the quiet condition). However, after the process of GPSTEC assimilation, the RMSE

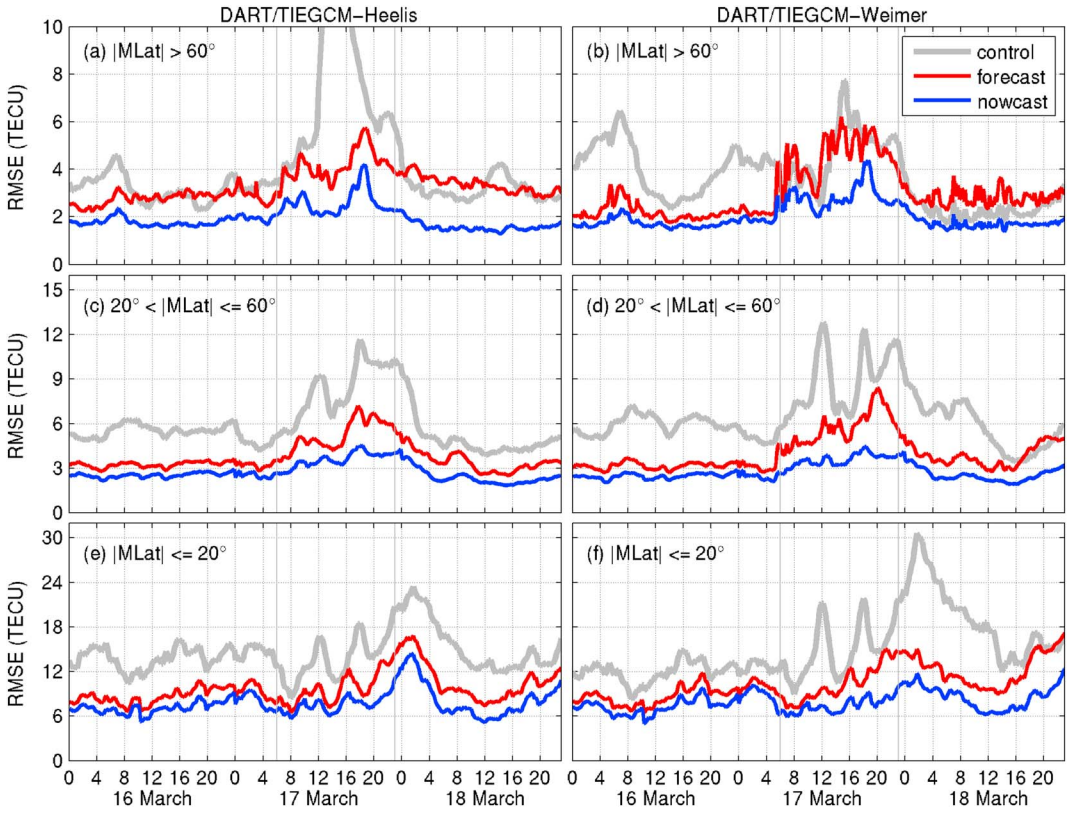

Figure 3. The time series of RMSE by (a, c, and e) DART/TIEGCM-Heelis and (b, d, and f) DART/TIEGCM-Weimer modes at magnetic high-latitude region (Figures 3a and 3b), midlatitude region (Figures 3c and 3d), and low-latitude region (Figures 3e and 3f). The gray line indicates the control run result. The red and blue lines indicate the forecast and nowcast results, respectively. The gray vertical lines indicate the time at 0600 UT and 2300 UT, which the *Dst* index (Figure 1) reaches the maximum and minimum values, respectively.

range between the nowcast and the forecast by the DTW model become smaller than by the DTH model. Since the nowcast result is obtained by assimilating the observation into the forecast result at last time step, the small range between nowcast and forecast indicates the small adjustment in the assimilation. This implies that the assimilation scheme of DTW model is more suitable for the model forecast at the high-latitude region during this period. After 0500 UT, the forecast RMSE (red line) by the DTW model is suddenly increasing and its variation becomes rapid vibration during the storm main phase. Again, the forecast RMSE by the DTW model has the suddenly enhancement at 1200 UT, the time when the *Dst* index reaches its second peak during the storm main phase (Figure 1). This feature is unclear at the case of DTH model. After 2300 UT, the DTW forecast RMSEs become smaller than the DTH forecast RMSEs during the storm recovery phase but still have larger RMSEs than the control run RMSEs. The variations of midlatitude RMSEs (nowcast and forecast) by the DTH (Figure 3c) and the DTW (Figure 3d) models are very similar, but the DTW forecast RMSEs have larger values than the DTH forecast RMSEs after 1600 UT on 18 March (recovery phase). At the low-latitude region, the DTW control RMSEs in Figure 3f increase suddenly after the storm main phase but are significantly reduced by assimilating the GPSTEC observations (blue line). The DTW forecast RMSE raise again after 1600 UT on 18 March.

Figure 4 shows the neutral parameters (neutral temperature and horizontal neutral winds) by control run and the forecast results in the DART/TIEGCM assimilation system at the midlatitude region. Results show that the neutral temperature increases during the storm main phase and then reduce during the storm recovery phase by the DTH and the DTW models. The meridional neutral winds (Figures 4b and 4c) show strongest equatorward wind around 1500–1600 UT by the DTW model. This equatorward wind during the main phase of St. Patrick's Day storm has been reported by the observational paper [*Tulasi Ram et al.*, 2016]. The zonal neutral wind assimilated by the DTW model is also similar to the observations. Although the model

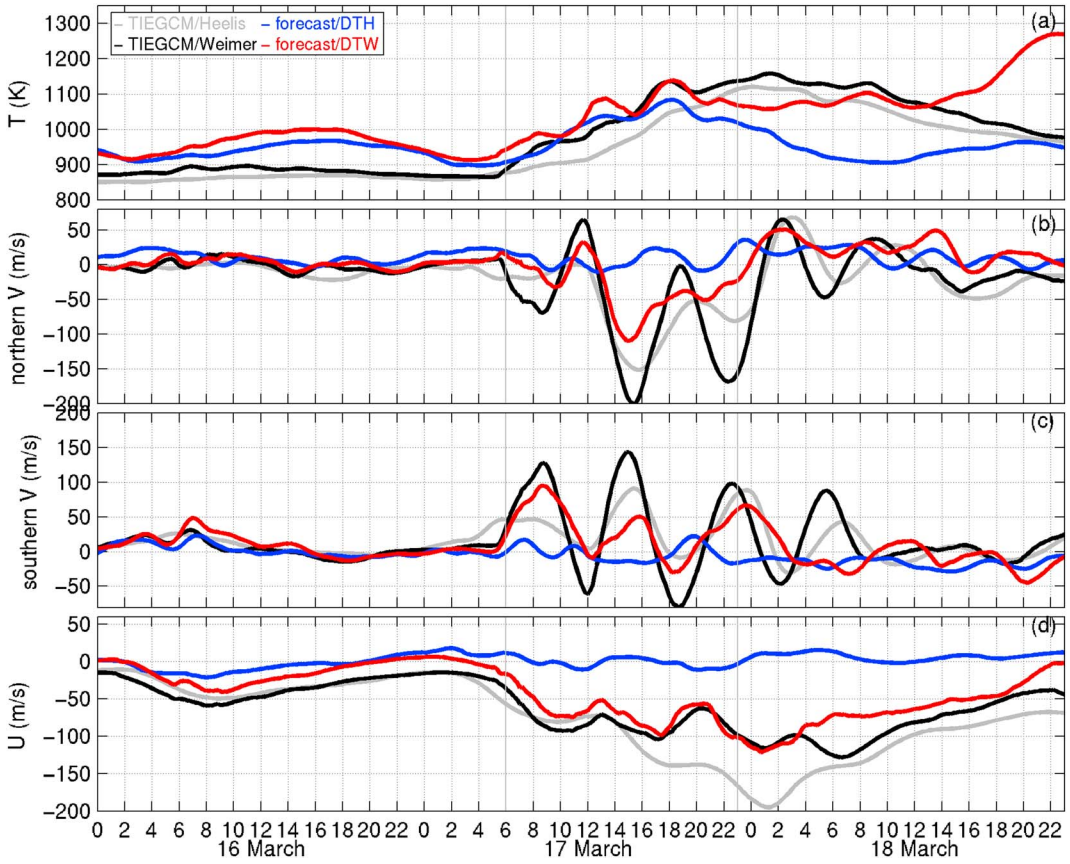

Figure 4. Time evolution of (a) averaged neutral temperature, (b) meridional neutral wind in the Northern Hemisphere, (c) meridional neutral wind in the Southern Hemisphere, and (d) zonal neutral wind at the magnetic midlatitude region. The gray and black lines are the control run with Heelis and Weimer models, respectively. The blue and red lines are the forecast stage of assimilation model.

assimilation results are smaller than the observation, the feature of wind directions is correct. However, the neutral winds assimilated by the DTH model have the opposite directions in respect to the observations.

2.2. TEC Forecast During Storm Period

In order to evaluate the forecast capability of the DTH and the DTW models during the 2015 St. Patrick's Day storm event, we further run the 24 h TEC forecast at every hour during 16–18 March and then compare the results with the GPSTEC observation. The 24 h TEC forecast is run by the TIEGCM-Heelis (TIEGCM-Weimer) model with the realistic parameters ($F_{10.7}$, *Kp*, IMF, or solar wind conditions) and the initial condition for each 24 h forecast is obtained from the nowcast results. The RMSE are divided by the GPSTEC values (referred to as "RMSE ratio" henceforth) in three different magnetic latitude regions to diminish the latitudinal difference in TEC value. Note that the definition of three regions is the same as Figure 3. The high-latitude (low-latitude) region is defined as the region that magnetic latitude larger (lower) than 60° (20°) in two hemispheres. The midlatitude is defined as the region between high-latitude and low-latitude regions. Figure 5 shows the 24 h forecast of RMSE ratio by the DTH model. It is clearly seen that the RMSE ratios at the high-latitude region are larger than those at the middle- and the low-latitude regions, especially during the magnetic storm main phase. The high RMSE ratios at the high-latitude region reduce after the storm recovery phase but still much larger than those at other regions. At the midlatitude region, the high RMSE ratios mainly appear during the storm main phase and reduce again during the storm recovery phase. At the low-latitude region, the maximum value of RMSE ratio appear around the storm main phase, but the value is relatively low comparing with the maximum values at the other regions. Figure 6 further shows the 24 h forecast of RMSE ratio by the DTW model. Compared with the results by the DTH model, the high-latitude RMSE ratios become small and the high RMSE ratios are mainly concentrated at the period of storm main phase. On the contrary, the RMSE ratios

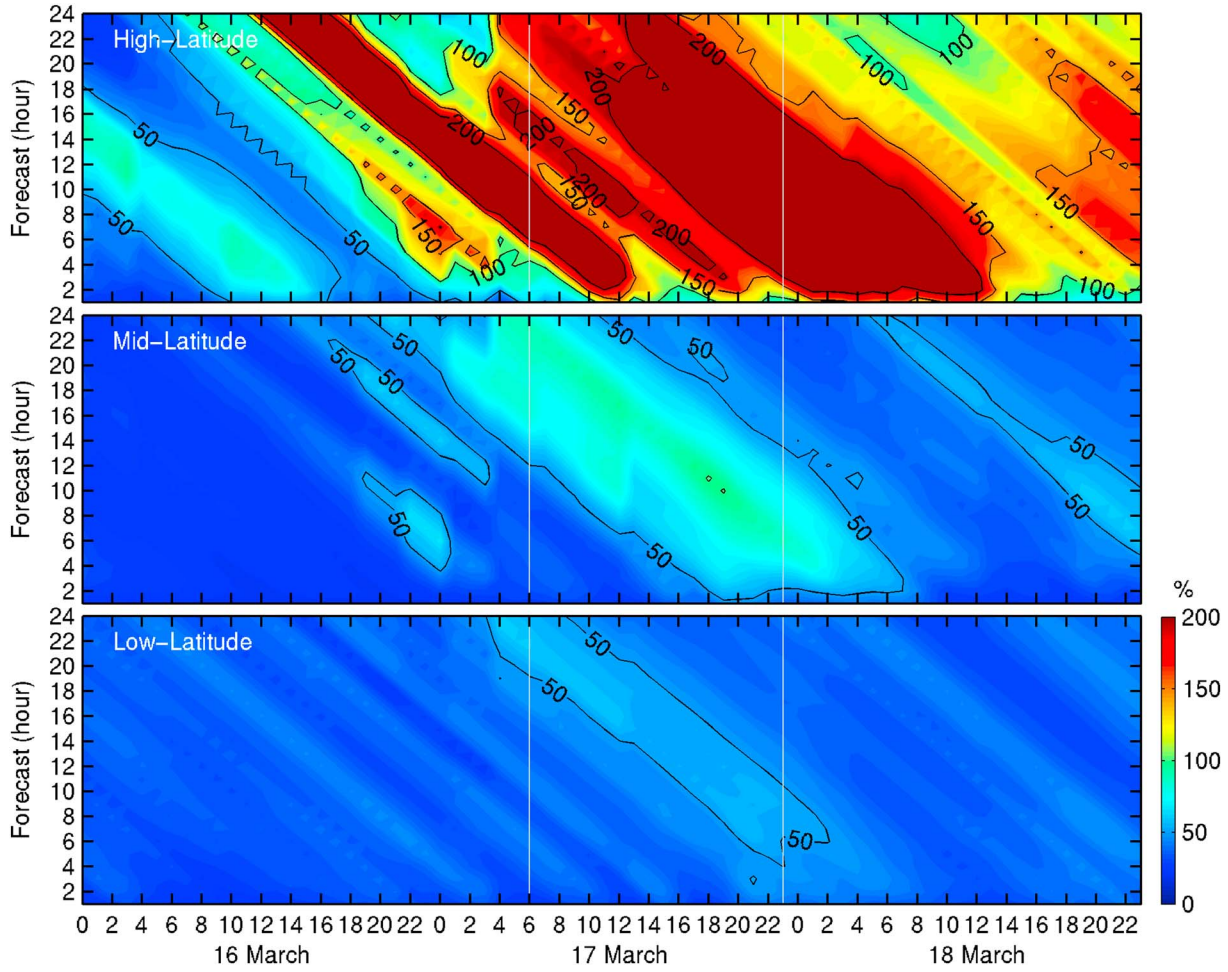

Figure 5. The ratio of RMSE over GPSTEC values for 24 h forecast period by DART/TIEGCM-Heelis model in three different magnetic latitude regions. The high-latitude (low-latitude) region is defined as the region that magnetic latitude larger (lower) than 60° (20°) in two hemispheres. The midlatitude is defined as the region between high-latitude and low-latitude regions. The white vertical lines indicate the time at 0600 UT and 2300 UT, which the *Dst* index (Figure 1) reaches the maximum and minimum values, respectively.

by the DTW model are slightly larger than those by the DTH model at the middle- and the low-latitude regions. It is important to note that, in the case of DTW model, a relatively high RMSE ratio appears at the low-latitude region during the storm recovery phase.

The limit of predictability of deterministic forecast is defined as the time when the forecast error reaches 95%, 71%, and 50% [*Lorenz*, 1969; *Savijärvi*, 1995]. In this study, we use the symbols $\tau_{95\%}$, $\tau_{71\%}$, and $\tau_{50\%}$, respectively. The time limit $\tau_{71\%}$ is the time when the forecast error exceeds $1/\sqrt{2}$ of the RMSE ratio. Figure 7 presents the time variations of time limit in hours by the DTH and the DTW models. At the high-latitude region, it is clearly seen that the time limits in the case of DTH model become short when the time approaching to the storm occurrence. The time of forecast capability is close to 0 h during the whole magnetic storm period. On the other hand, in the case of DTW model, the time limits are also getting close to 0 h when the time approaching to the storm occurrence but have the longer time limits comparing with the DTH time limits. It is noted that the time limit $\tau_{95\%}$ of DTW model (black line in Figure 7b) increases after 1200 UT on 18 March (recovery phase) but rapidly change with time. The time limits in the mid- and the low-latitude regions have different features with those in the high-latitude region. At the mid-latitude region, the time limits, $\tau_{50\%}$ and $\tau_{71\%}$, by DTH model reduce their values before the occurrence of storm. The minimum time limit $\tau_{95\%}$ is 8 h during the storm main phase in the case of DTH model. The DTW model has the slightly longer time limits of $\tau_{50\%}$ and $\tau_{71\%}$ but has the shorter time limit of $\tau_{95\%}$ comparing with the DTH model. The

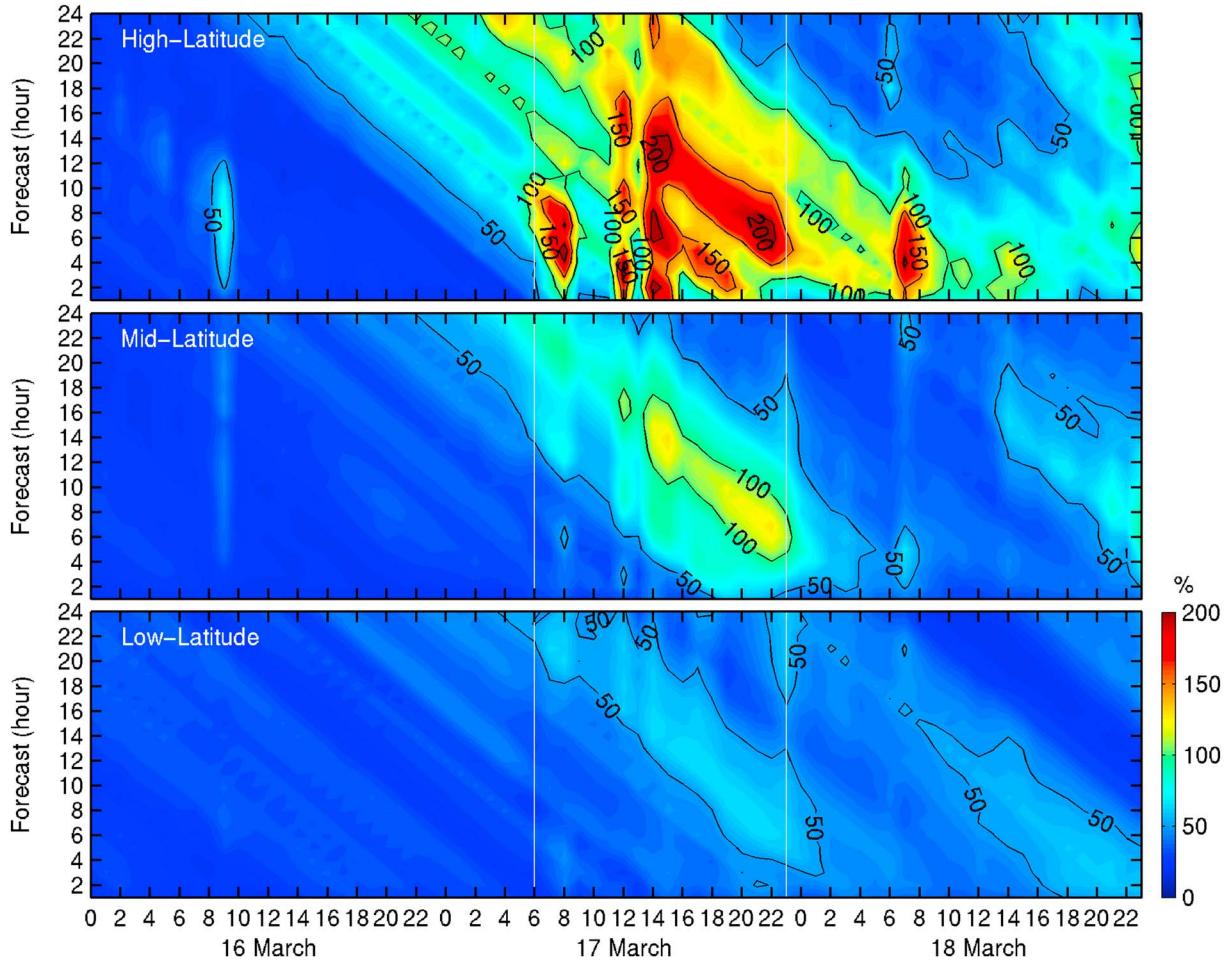

Figure 6. The same format as Figure 5 but for the case of DART/TIEGCM-Weimer model.

minimum time limit $\tau_{95\%}$ is 3 h during the storm main phase in the DTW model. At the low-latitude region, the feature of time limit $\tau_{50\%}$ is similar for the DTH and the DTW models during the storm main phase. However, the time limit $\tau_{50\%}$ by the DTW model becomes short again and close to 0 h during the storm recovery phase.

3. Discussion

As presented in Figure 2, the global TEC of control runs by both the TIEGCM-Heelis, and the TIEGCM-Weimer models underestimate the EIA strength in the Southern Hemisphere. Furthermore, the EIA structure is not reproduced well by the TIEGCM-Heelis model, which shows shorter EIA tail around dusk comparing with the GPSTEC observation. Also, the TIEGCM-Heelis model shows plasma enhancement region around the auroral oval, but the GPSTEC does not show this kind of enhancement region (second panels of Figure 2a). As a result, the control RMSE raises at the high-latitude region during the storm main phase (gray line in Figure 3a). After assimilating the GPSTEC observation, the strength as well as the structure of EIA become more closely to the observation. The plasma enhancement around auroral oval also vanished, and the poleward extension of tongue of ionization in the Southern Hemisphere is further reproduced by the DTH model (fourth panel of Figure 2a).

On the other hand, the global EIA by the TIEGCM-Weimer model (control run in the second panel of Figure 2b) is relatively similar to the observation comparing with the TIEGCM-Heelis model. The assimilated TEC by the DTW model shows great improvement from the control run and has the smallest RMSE value after assimilation (blue lines in Figures 3b, 3d, and 3f). Furthermore, the forecast TEC (third panel in Figure 2b) by the DTW model shows clear SED structure in the Northern Hemisphere and the poleward extension of ionization in

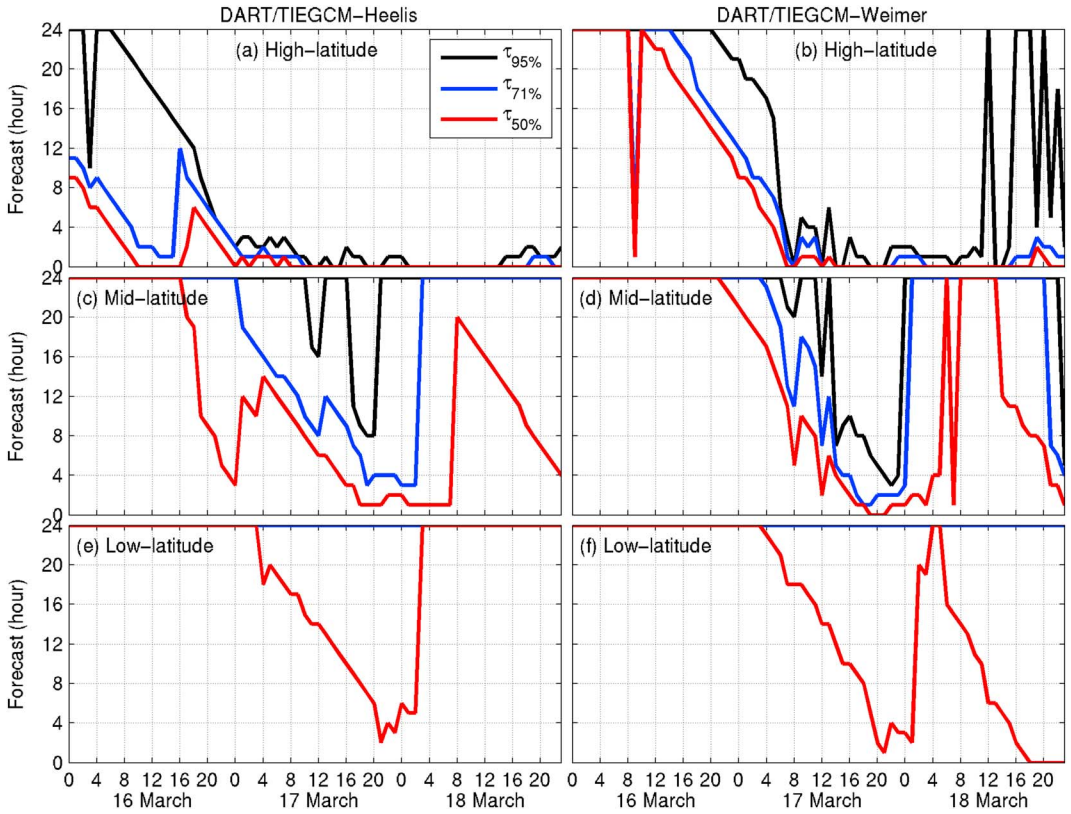

Figure 7. Time variations of the time limits $\tau_{95\%}$ (black line), $\tau_{71\%}$ (blue line), and $\tau_{50\%}$ (red line) in hours by (a, c, and e) the DTH and (b, d, and f) the DTW models.

the Southern Hemisphere, but the DTH model do not successfully forecast the clear SED structure. This result suggests that the DTW model can get the relatively correct trajectory of model forecasting during the storm period comparing with the DTH model, especially at the high-latitude region. However, both models underestimate the strength of southern EIA in the forecast during the 2015 St. Patrick's Day storm event.

In order to evaluate the model capability on the TEC forecast, we calculate the RMSE value by the TEC difference between the model results and the realistic TEC observations. In this study, we further separate the RMSEs in three different magnetic latitude region to discuss the latitudinal effect on the TEC forecasts by the DTH and the DTW models. Results show that these two models have clearly difference at the high-latitude region, which is caused by the different high-latitude ion convection obtained by these two models. For the case of 2015 St. Patrick's Day storm, the TIEGCM-Weimer model has smaller RMSEs than the TIEGCM-Heelis model during the storm period (gray lines in Figures 3a and 3b). Since the ionospheric electron density changes rapidly during the storm, these smaller RMSEs may be contributed by the frequently updating (5 min) the forcing parameters (solar wind and IMF) in the TIEGCM-Weimer model. The TIEGCM-Heelis model with 3 h resolution of *Kp* index may not be able swiftly adapt to ionospheric storm effects with time scales shorter than 3 h. The short assimilation cycling, 10 min in this study, can help the physical model to track the rapid variations during the storm time event for the fixed forcing parameters [*Chen et al.*, 2016]. As a result, the RMSEs at the high-latitude (blue lines in Figures 3a and 3b) become smaller than the control cases, resulting in a great improvement in the nowcast.

The reproduction of longer tail of EIA around dusk by data assimilation model is also an interesting topic in this study. This feature is caused by the prereversal enhancement to uplift the lower altitude electron density to a higher altitude and result in a longer life time of electron density. Figure 8 shows the global distributions of eastward electric field at a constant pressure surface (~235 km altitude) as well as the TEC by the control runs (top row) and the assimilation forecast (bottom row). Noted that the electric field is calculated by the special differentiation of the potential. Results show that the control TEC by the TIEGCM-Weimer model

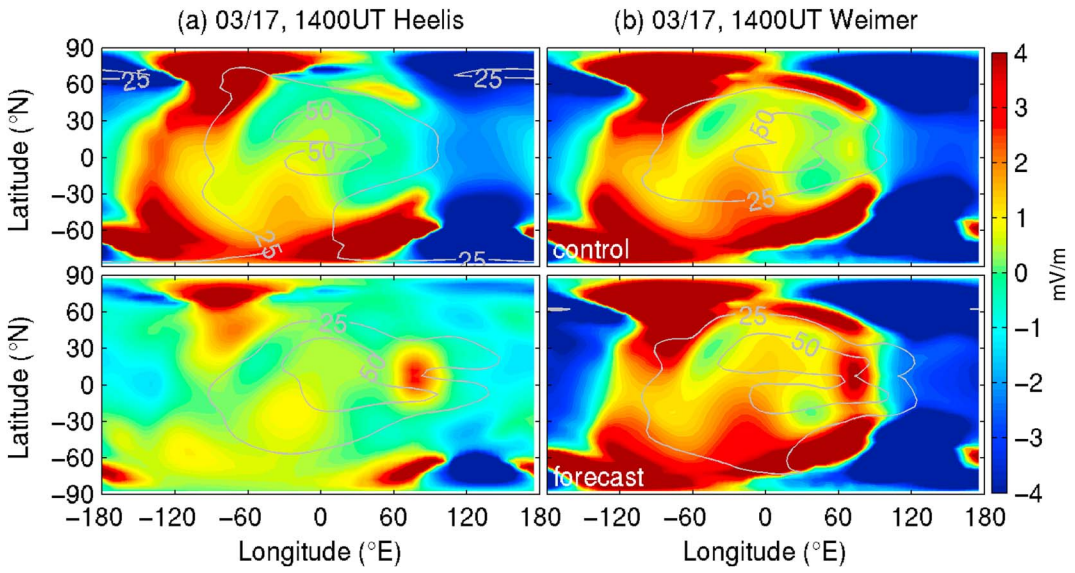

Figure 8. The global eastward electric field and the TEC at 1400 UT on 17 March 2015. (a) The results by the control run from TIEGCM-Heelis model (top) and the forecast from DART/TIEGCM-Heelis model (bottom). (b) The results by the control run from TIEGCM-Weimer model (top) and the forecast from DART/TIEGCM-Weimer model (bottom). The color is the global electric field (positive eastward), and the gray line indicates the TEC contour.

(top of Figure 8b) has slightly separation of EIAs in the latitude at the evening sector (around geographic longitude of 60°E). The TEC by the TIEGCM-Heelis model (top of Figure 8a), however, does not show clear EIA separation at the evening sector. One of the reasons may be the different eastward electric fields around the evening sector by these two models, showing slightly eastward (~1 mV/m) in the TIEGCM-Weimer model and ~0 mV/m in the TIEGCM-Heelis model. After assimilating the GPSTEC observations, the resulting electric field and TEC are shown in the bottom of Figures 8a and 8b. It is seen that the clearly separation of EIA crests appear and further extend to the premidnight sector for the DTH and the DTW models. Compared with the control runs, the eastward electric fields are enhanced by these two assimilation models around the evening sector. Since the potential is not the state variable in the assimilation system, the variations of electric field may be due to the adjustment of electron density in the model, which has the different gradient of electron density and then reflects to the gradient of conductivity. As a result, the enhancement of eastward electric field appears around the trough of EIAs (bottom of Figures 8a and 8b) around dusk. The eastward electric field then induce the vertical plasma drift and uplift the plasma to a higher altitude and cause the separation of EIA crests in the assimilation model. The effect of the vertical drift in modification of the EIA crests during quiet and storm periods have been reported by several observational, statistical, and theoretical studies [e.g., *Rastogi and Klobuchar*, 1990; *Chen et al*., 2008; *Lin et al*., 2009; *Stoneback et al*., 2013]. The feature of strong vertical drift in this assimilation model around Indian sector at 1400 UT on 17 March 2015 has been confirmed by the observational results reported by *Joshi et al*. [2016]. Our results suggest that the estimated electric fields in the ionospheric assimilation system have good agreement with the observations, even we only assimilate the GPSTEC observations.

The 24 h forecast results (Figures 5–7) shows that the capability of TEC forecast is better at the low-latitude region than that at the middle- and high-latitude regions. The time limit in Figure 7 further presents the limitation of model predictability by the DTH and the DTW models. Results show it is difficult to forecast the high-latitude TEC during the 2015 St. Patrick' Day storm for both forecast models. It is noted that the data coverage in the high-latitude region is better than the low- and middle-latitude regions (the first panels of Figures 2a and 2b). This suggests that the difficulty of high-latitude forecast may not come from the data coverage. We suspect that the driving forces in high latitudes from magnetosphere, currents, and electric fields have less correlation with electron density (GPSTEC). The time limits become longer at the low-latitude region but still have shorter forecast time during the period of storm main phase comparing with the quiet day (16 March) and the period of storm recovery phase (18 March), except the time limit $\tau_{50\%}$ by the DTW

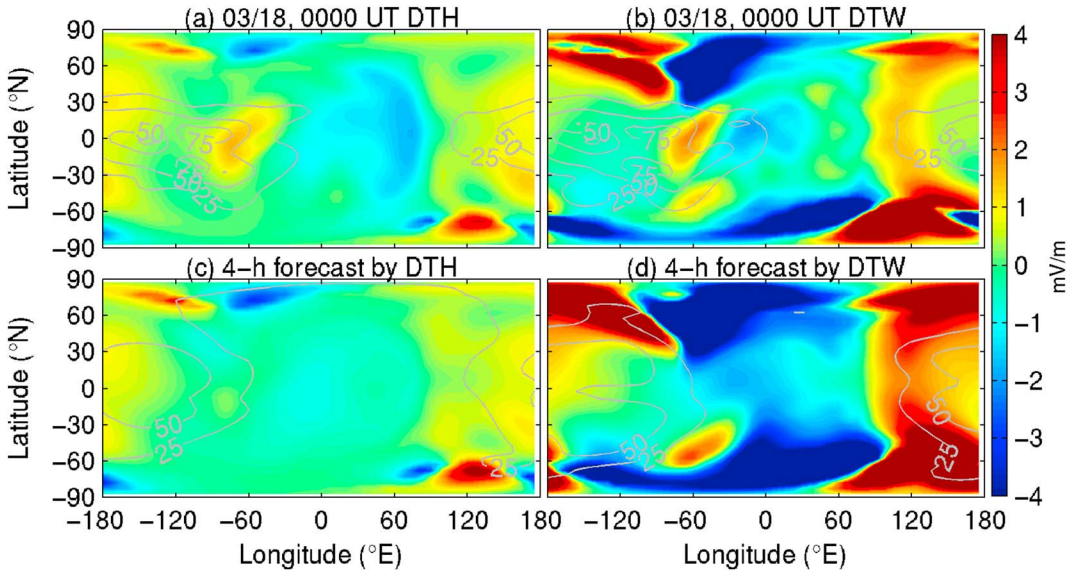

Figure 9. The comparison between (a, b) the assimilation and (c, d) the 4 h forecast results in global electric field (color contour) and TEC (gray line contour). Figures 9a and 9c are the results by the DART/TIEGCM-Heelis model, while Figures 9b and 9d are the results by the DART/TIEGCM-Weimer model. The positive value in electric field indicates the eastward electric field.

model. Figure 9 shows the 4 h forecast results and their comparison with the assimilation results of the electric field and the TEC at 0000 UT on 18 March 2015. Note that the 4 h forecast at 0000 UT on 18 March is calculated by the initial conditions at the time of 2000 UT on 17 March. This is the time near the minimum $\tau_{50\%}$ at the low-latitude region during the storm main phase (Figures 7e and 7f). The assimilation results in Figures 9a and 9b are calculated by the initial conditions at the previous time step (2350 UT on 17 March) and then assimilated by the GPSTEC observations (see section 2.1). Since the frequently updating let the assimilation model can restrain the unrealistic model error [*Chen et al.*, 2016], the assimilation results are seen as the reference for evaluating the 4 h forecast. Both DTH and DTW models show the clearly enhancement of eastward electric field at low-latitude region around geographic longitude of −60°E (Figures 9a and 9b). The 4 h forecasts shown in Figures 9c and 9d, however, do not show the clear eastward electric field at the same region. As a result, the EIA crests disappear fast at the evening sector and lead to different structure from the assimilation results of Figures 9a and 9b. Therefore, it is suggested that the electric field is an important factor to affect the accuracy of TEC forecast during the storm main phase, especially at the low-latitude region. In the future, the electric fields as well as the vertical plasma drift observed by satellites will be further assimilated in this ionospheric assimilation system to obtain a better accuracy of ionospheric forecast.

4. Conclusion

In this study, we assimilate the ground-based GPSTEC observations into the TIEGCM model and further evaluate its performances during the 2015 St. Patrick' Day geomagnetic storm. The RMSEs between the model TECs and the true observations are divided into three different regions by the magnetic latitude to discuss the latitudinal effect on the TEC forecast by the ionospheric assimilation system. The capability of TEC forecast is also evaluated by performing the 24 h forecast. The main results in this study are listed as follows:

1. The time variations of RMSE in Figure 3 show the DTW model has better accuracy of TEC forecast comparing with the DTH model, especially at the high-latitude region.
2. The equatorward and zonal neutral winds during the storm main phase are adjusted by the DTW model to approach the observations. However, the neutral winds assimilated by the DTH model have the opposite directions in respect to the observations.
3. Twenty-four hour forecast results in Figure 7 indicate that the forecast time is longer at the low-latitude than other latitudes.

4. The eastward electric field is also adjusted by the assimilation model. As a result, the feature of eastward electric field is improved to access to the observations around the evening sector during the storm main phase.
5. The comparison between the 4 h forecast and the assimilation results suggests the assimilation of the electric field or the vertical plasma drift is important to improve the capability of ionospheric model forecast.

Acknowledgments
This paper is supported by Ministry of Science and Technology (MOST) and National Space Organization (NSPO) of Taiwan to National Cheng Kung University under MOST-105-2111-M-006-003, MOST-105-2111-M-006-008, MOST-103-2923-M-006-002-MY3, and NSPO-S-105120. T.M. is supported by NASA award NNX14AI17G and AFOSR award FA9550-13-1-0058. The source code for the assimilation system and simulation model used in this study, the DART and TIE-GCM, is available at http://www.image.ucar.edu/DAReS/DART/ and http://www.hao.ucar.edu/modeling/tgcm/, respectively. The observations data from ground-based GPS receivers are available at IGS (https://igscb.jpl.nasa.gov/components/data.html). The authors are grateful for the NCAR High Altitude Observatory and Data Assimilation Research Section for their support of TIE-GCM and DART software.

References

Anderson, J. L., T. Hoar, K. Raeder, H. Liu, N. Collins, R. Torn, and A. F. Arellano (2009), The Data Assimilation Research Testbed: A community data assimilation facility, *Bull. Am. Meteorol. Soc.*, *90*, 1283–1296, doi:10.1175/2009BAMS2618.1.

Astafyeva, E., I. Zakharenkova, and M. Förster (2015), Ionospheric response to the 2015 St. Patrick's Day storm: A global multi-instrumental overview, *J. Geophys. Res. Space Physics*, *120*, 9023–9037, doi:10.1002/2015JA021629.

Chartier, A. T., D. R. Jackson, and C. N. Mitchell (2013), A comparison of the effects of initializing different thermosphere-ionosphere model fields on storm time plasma density forecasts, *J. Geophys. Res. Space Physics*, *118*, 7329–7337, doi:10.1002/2013JA019034.

Chartier, A. T., T. Matsuo, J. L. Anderson, N. Collins, T. J. Hoar, G. Lu, C. N. Mitchell, A. J. Coster, L. J. Paxton, and G. S. Bust (2016), Ionospheric data assimilation and forecasting during storms, *J. Geophys. Res. Space Physics*, *121*, 764–778, doi:10.1002/2014JA020799.

Chen, C. H., J. Y. Liu, K. Yumoto, C. H. Lin, and T. W. Fang (2008), Equatorial ionization anomaly of the total electron content and equatorial electrojet of ground-based geomagnetic field strength, *J. Atmos. Sol. Terr. Phys.*, *70*, 2172–2183, doi:10.1016/j.jastp.2008.09.021.

Chen, C. H., C. H. Lin, T. Matsuo, W. H. Chen, I. T. Lee, J. Y. Liu, J. T. Lin, and C. T. Hsu (2016), Ionospheric data assimilation with thermosphere-ionosphere-electrodynamics general circulation model and GPS-TEC during geomagnetic storm conditions, *J. Geophys. Res. Space Physics*, *121*, 5708–5722, doi:10.1002/2015JA021787.

Cherniak, I., and I. Zakharenkova (2015), Dependence of the high-latitude plasma irregularities on the auroral activity indices: a case study of 17 March 2015 geomagnetic storm, *Earth Planets Space*, *67*, 151, doi:10.1186/s40623-015-0316-x.

Fuller-Rowell, T. J., C. F. Minter, and M. V. Codrescu (2004), Data assimilation for neutral thermospheric species during geomagnetic storms, *Radio Sci.*, *39*, RS1S03, doi:10.1029/2002RS002835.

Heelis, R. A., J. K. Lowell, and R. W. Spiro (1982), A model of the high latitude ionosphere convection pattern, *J. Geophys. Res.*, *87*, 6339–6345, doi:10.1029/JA087iA08p06339.

Jacobsen, K. S., and Y. L. Andalsvik (2016), Overview of the 2015 St. Patrick's day storm and its consequences for RTK and PPP positioning in Norway, *J. Space Weather Space Clim.*, *6*, A9, doi:10.1051/swsc/2016004.

Jee, G., A. G. Burns, W. Wang, S. C. Solomon, R. W. Schunk, L. Scherliess, D. C. Thompson, J. J. Sojka, and L. Zhu (2007), Duration of an ionospheric data assimilation initialization of a coupled thermosphere-ionosphere model, *Space Weather*, *5*, S01004, doi:10.1029/2006SW000250.

Joshi, L. M., S. Sripathi, and R. Singh (2016), Simulation of low-latitude ionospheric response to 2015 St. Patrick's Day super geomagnetic storm using ionosonde-derived PRE vertical drifts over Indian region, *J. Geophys. Res. Space Physics*, *121*, 2489–2502, doi:10.1002/2015JA021512.

Lin, C. H., A. D. Richmond, J. Y. Liu, G. J. Bailey, and B. W. Reinisch (2009), Theoretical study of new plasma structures in the low-latitude ionosphere during a major magnetic storm, *J. Geophys. Res.*, *114*, A05303, doi:10.1029/2008JA013951.

Lorenz, E. N. (1969), The predictability of flow which possesses many scale of motion, *Tellus*, *21*, 289–307, doi:10.1111/j.2153-3490.1969.tb00444.x.

Nava, B., J. Rodriguez-Zuluaga, K. Alazo-Cuartas, A. Kashcheyev, Y. Migoya-Orué, S. M. Radicella, C. Amory-Mazaudier, and R. Fleury (2016), Middle- and low-latitude ionosphere response to 2015 St. Patrick's Day geomagnetic storm, *J. Geophys. Res. Space Physics*, *121*, 3421–3438, doi:10.1002/2015JA022299.

Rastogi, R. G., and J. A. Klobuchar (1990), Ionospheric electron content within the equatorial F_2 layer anomaly belt, *J. Geophys. Res.*, *95*, 19,045–19,052, doi:10.1029/JA095iA11p19045.

Savijärvi, H. (1995), Error growth in a large numerical forecast system, *Mon. Weather Rev.*, *123*, 212–221, doi:10.1175/1520-0493(1995)123<0212:EGIALN>2.0.CO;2.

Solomentsev, D., K. S. Jacobsen, B. Khattatov, V. Khattatov, Y. Cherniak, and A. Titov (2014), Ionosphere data assimilation capabilities for representing the high-latitude geomagnetic storm event in September 2011, *J. Geophys. Res. Space Physics*, *119*, 10,581–10,594, doi:10.1002/2014JA020248.

Stoneback, R. A., N. K. Malakar, D. J. Lary, and R. A. Heelis (2013), Specifying the equatorial ionosphere using CINDI on C/NOFS, COSMIC, and data interpolating empirical orthogonal functions, *J. Geophys. Res. Space Physics*, *118*, 6706–6722, doi:10.1002/jgra.50596.

Tulasi Ram, S., et al. (2016), Duskside enhancement of equatorial zonal electric field response to convection electric fields during the St. Patrick's Day storm on 17 March 2015, *J. Geophys. Res. Space Physics*, *121*, 538–548, doi:10.1002/2015JA021932.

Weimer, D. R. (2005), Improved ionospheric electrodynamic models and application to calculating Joule heating rates, *J. Geophys. Res.*, *110*, A05306, doi:10.1029/2004JA010884.